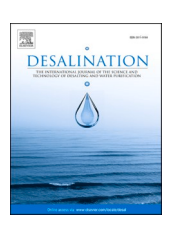
ELSEVIER

Contents lists available at ScienceDirect

Desalination

journal homepage: www.elsevier.com/locate/desal





Cyclic simulation and energy assessment of closed-circuit RO (CCRO) of brackish water

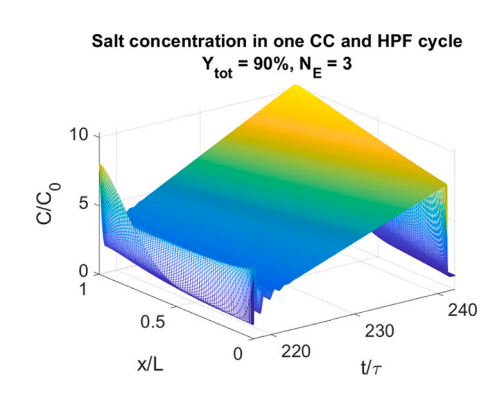
Mingheng Li

Department of Chemical and Materials Engineering, California State Polytechnic University, Pomona, CA 91768, USA

HIGHLIGHTS

- Spatiotemporal models are developed to couple filtration and flushing in cyclic operation of CCRO.
- High pressure flushing and low pressure flushing are compared.
- Contributing factors to SEC in CCRO of brackish water are ranked.
- CCRO and multi-stage RO are compared in terms of energy performance.

GRAPHICAL ABSTRACT



ARTICLE INFO

Keywords: CCRO Process dynamics System analysis Partial differential equation Specific energy consumption

ABSTRACT

A previously developed spatiotemporal model is enhanced to simulate detailed dynamic and cyclic behavior of closed-circuit RO (CCRO). The partial differential equation (PDE) model couples water balance, salt balance and momentum balance and explicitly accounts for pressure drop, concentration polarization and axial dispersion in both closed-circuit (CC) and flushing modes. Simulation case studies using conditions similar to those in a well-studied industrial brackish water plant were carried out and the specific energy consumption (SEC) in CCRO at the cyclic steady state (CSS) was analyzed from thermodynamic restriction, flux requirement, flow resistance, concentration polarization and salt retention. On the basis of the same flux used in industrial conditions, CCRO is not as energy efficient as state-of-the-art multi-stage RO for low-salinity brackish water desalination. Operating CCRO at a reduced flux can make it competitive.

1. Introduction

Desalination offers a viable solution to clean water production from saline and brackish groundwater resources [1–3]. Among all industrial desalination techniques, reverse osmosis (RO) membrane separation is by far the most widely adopted one, accounting for approximately 70 %

of the desalinated water produced worldwide [4].

Traditionally, RO membrane processes are operated at steady state. The cross-flow pattern in commercial spiral wound membranes is featured with unbalanced flux, which adversely affects energy efficiency in seawater RO (SWRO) [5]. Specific energy consumption (SEC) is an important research topic in SWRO because the energy consumption

E-mail address: minghengli@cpp.edu.

accounts for a major portion of total production cost [6]. Energy recovery devices (ERDs) are indispensable in modern SWRO plants, which can recover 97 % of the hydraulic energy in the high-pressure brine [7]. Increasing membrane area and/or using ultra permeable membranes may save energy costs, but only to a certain extent, as exhibited by "a law of diminishing returns" [8]. Another strategy to reduce the SEC is via improved membrane designs and operations [9]. For example, staged design in conjunction with interstage booster pump(s) enable a more uniform driving force along the process, therefore improving energy efficiency [10-12]. Most recently, novel semi-batch RO (SBRO) [13-20] and batch RO (BRO) [5,17,20,21] have been studied. SBRO has been patented by Desalitech (now part of DuPont) under the name closed-circuit RO (CCRO). In these designs, a temporally varying pressure is applied, mimicking the spatially varying pressure used in continuous multi-stage ROs with booster pumps. It has been shown that in an ideal situation, the SEC in BRO can approach the thermodynamic minimum [5,17,22]. Other benefits include reduced fouling risk in lead elements due to a relatively uniform flux [23] and periodic flushing of membrane which may facilitate foulant removal. CCRO is also known for its operational flexibility; a wide range of water recovery levels can be achieved by adjusting the filtration and flushing time periods [19].

In inland areas, many desalination facilities are actively looking

beyond conventional ROs to increase the system recovery to 90 % or higher aiming for increased water production and reduced brine disposal. At high recoveries, scaling of sparingly soluble minerals becomes a concern [24,25]. Both BRO and CCRO have been suggested in literature for energy-efficient, high-recovery wastewater and brackish water RO (BWRO) applications. Pilot testings of CCRO have been or are being conducted by various wastewater and brackish water desalination facilities including several in Southern California [26–28]. There is still debate concerning the potential advantage of CCRO over conventional steady-state RO. In a recent work, Cohen and coworkers pointed out that cycle-to-cycle salt buildup in CCRO under realistic operating conditions could severely impact its energy performance [19]. Flow reversal RO (FRRO) is another non-conventional RO proposed for high recovery BWRO operation as it may reset the "crystallization induction clock" [29-34]. In early 2022, City of Santa Monica announced the plan to build the first FRRO municipal desalination plant in the United States [35], confirming the promise and potential of this emerging technology. Pulse flow RO (PFRO) has also been proposed [36]. It uses short and rapid pulses with high shear force to prevent membranes from fouling even at high recoveries.

BRO, SBRO, FRRO and PFRO all belong to the class of *dynamic and cyclic RO* where process variables are functions of time and space. A

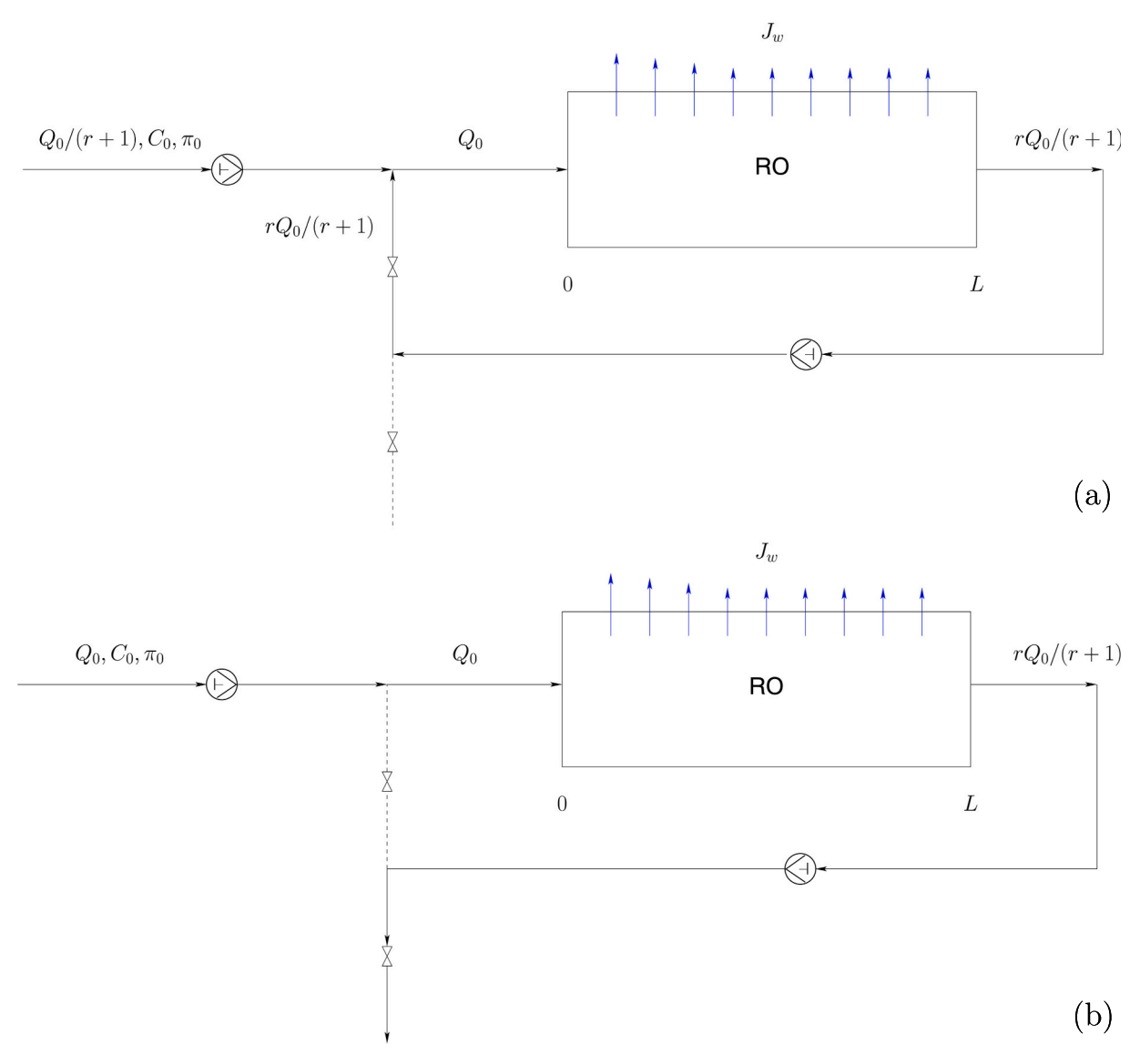


Fig. 1. Schematic of (a) closed-circuit mode and (b) high pressure flushing mode of CCRO. $r=(1-Y_{SP})/Y_{SP}$.

characterization of spatiotemporal behavior of hydrodynamics and mass transfer entails partial differential equations (PDEs) [37]. Moreover, the processes have filtration and flushing/refilling steps that are coupled together and will eventually converge to a cyclic steady state (CSS) largely independent of the initial state. This work leverages current knowledge and practices on pressure-swing adsorption (PSA), a mature industrial technology for gas separations [38], for studying the cyclic dynamics of CCRO and its performance at the CSS. The ultimate goal is to develop a unified computational framework for model-based design and optimization of dynamic and cyclic membrane processes.

2. Mathematical model

A schematic of CCRO is shown in Fig. 1. Each cycle consists of closed-circuit (CC) and flushing steps. In the CC mode, the permeate and the fresh feed have the same flow rate (Q_p) , or 100 % recovery. The concentrate is recycled in the closed circuit to maintain a time-invariant total feed (Q_0) .

The single pass recovery is defined as:

$$Y_{SP} = \frac{Q_p}{Q_0} \tag{1}$$

The recycle to raw feed ratio in the CC mode (r) is calculated as follows:

$$r = \frac{Q_c}{Q_p} = \frac{1 - Y_{SP}}{Y_{SP}} \tag{2}$$

where Q_c is the concentrate rate.

Membrane manufacturers recommend recovery per element to be limited to a low level (15 % or less [19]). If $Y_{SP} = 10\%$ (for one single element per vessel in CCRO), r=9.

Because of salt accumulation in the CC step, the system must be flushed occasionally before the next filtration step. In the flushing mode, the valve for recycle operation is turned off, and the concentrate is allowed to leave the system. The fresh feed rate is increased such that the same Q_0 is maintained at the entrance of the RO. In addition to high pressure flushing (HPF) shown in Fig. 1, where the recovery is Y_{SP} , there is also low pressure flushing (LPF), where no permeate is produced during flushing. In both cases, the filtration/flushing time ratio dictates the total recovery Y_{tot} [19]:

$$Y_{tot} = \frac{Y_{SP}(t_{FT}/t_{FL}) + \delta Y_{SP}}{Y_{SP}(t_{FT}/t_{FL}) + 1}$$
(3)

where δ =1 for HPF and 0 for LPF.

If $Y_{tot} = 90\%$ and $Y_{SP} = 10\%$, it can be verified that $t_{FT}/t_{FL} = 80$ for HPF and $t_{FT}/t_{FL} = 90$ for LPF.

For a fair comparison among conventional steady-state RO, CCRO with LPF (CCRO-LPF) and CCRO with HPF (CCRO-HPF), the total raw intake rate, the total recovery rate and the total number of RO elements are all fixed. Under these conditions, the time-average flux (for a time period lasting one filtration and one flushing cycle) \overline{J}_w is the same in all cases.

Let \overline{Q}_f be the total feed rate divided by the total number of elements in conventional RO, Q_0 in CCRO can be calculated from the mass balance equation $N_E \overline{Q}_f(t_{FT} + t_{FL}) = (Q_0 Y_{SP}) t_{FT} + Q_0 t_{FL}$, where N_E is the number of elements per vessel in CCRO, or

$$Q_0 = \frac{N_E \overline{Q}_f(t_{FT} + t_{FL})}{Y_{SP}t_{FT} + t_{FL}} \tag{4}$$

The average water flux during CC filtration $\overline{J}_{w,FT}$ is dependent on Q_0 , or

$$\overline{J}_{w,FT} = \frac{Q_0 Y_{SP}}{A_m} \tag{5}$$

where A_m is the membrane area per vessel.

Because there is no flux during the flushing period of CCRO-LPF, both Q_0 and $\overline{J}_{w,FT}$ should be slightly higher than those in CCRO-HPF. The conditions for comparison between CCRO and three-stage RO at a 90 % recovery are summarized in Table 1. The number of elements per vessel and the number of vessels are varied in Section 3.1 to study their effect on process performance. Another case comparing CCRO with two-stage RO at an 81 % recovery is shown in Table 2. The multistage design conditions are based on a well-studied BWRO plant located in Chino, California, which has a feed TDS of about 950 mg/L. Mathematical models have been developed and validated against a wide range of operating and experimental conditions in this desalination facility [39–41].

The spatiotemporal model coupling water balance, salt balance, and momentum balance in dynamic RO has been derived in a published work [37]:

$$0 = \frac{\partial q^*}{\partial x^*} + \frac{\gamma_0}{1 + \frac{L_p \pi_0}{k_m} c^*} (\theta - c^*)$$

$$\frac{\partial c^*}{\partial t^*} = -q^* \frac{\partial c^*}{\partial x^*} - c^* \frac{\partial q^*}{\partial x^*} + \frac{1}{Pe_D} \frac{\partial^2 c^*}{\partial x^{*2}}$$

$$0 = \frac{\partial \theta}{\partial x^*} + \frac{a_2}{\pi_0} q^{*n_2}$$
(6)

where q^* is flow rate in the feed channel (Q) divided by its value at the entrance of RO (Q_0) . c^* is salt concentration (C) normalized by the concentration of the fresh feed (C_0). θ is the transmembrane pressure (ΔP) divided by the osmotic pressure of the fresh feed (π_0) . t^* is the actual time divided by the space time τ ($\tau = Q_0/V_c$, where V_c is the volume of the circuit). $x^* = x/L$ is the dimensionless length with 0 and 1 representing entrance and outlet of the RO stage respectively. L is the length of a pressure vessel, which is about 1 m for each RO element. γ_0 is a dimensionless parameter defined based on the combined feed rate and the osmotic pressure of the fresh feed, or $\gamma_0 = A_m L_p \pi_0/Q_0$ (A_m is membrane area per vessel and L_p is membrane hydraulic permeability). $k_m =$ $a_1q^{*n_1}$ is the mass transfer coefficient. Pe_D is the dispersive Peclet number. a_1 , n_1 , a_2 and n_2 are parameters that characterize mass transfer and pressure drop [41,42]. The model is based on the following assumptions: (1) the salt rejection of the membrane is 100 %, (2) the concentration polarization factor $CPF = \exp(J_w/k_m) \approx 1 + J_w/k_m$, and (3) the residence time distribution can be reasonably described by the dispersion model [42]. The parameters for one BW30-400 RO element per vessel are summarized in Table 3. These are derived from plant experiments and high-fidelity CFD simulations [41,42].

Table 1 Design conditions used for comparison between CCRO and three-stage RO at Y_{tot} = 90%.

	Three-stage RO	CCRO-HPF	CCRO-LPF
Total feed rate (m ³ /h)	346.4	346.4	346.4
Recovery	90 %	90 %	90 %
Feed osmotic pressure (bar)	0.62	0.62	0.62
RO array	$(28:14:7) \times 7$	343×1	343×1
Number of elements	343	343	343
RO element	BW30-400	BW30-400	BW30-400
Element area (m ²)	37	37	37
Membrane permeability (lmh/bar)	2.79	2.79	2.79
Average flux per element (lmh)	24.5	24.5	24.5 ^a
Filtration time to flushing time	00	80:1	90:1
Recovery per element	varies	10 %	10 %
Feed per vessel (m ³ /h)	12.4/9.5/8.0 ^b	9.1	9.2

^a 24.8 lmh during filtration and 0 during flushing.

 $^{^{\}rm b}$ This is based on design without booster pumps. With two inter-stage booster pumps, the flow per vessel at the entrance of each stage is 12.4, 10.8, and 9.3 m³/h, respectively [34].

Table 2 Design conditions used for comparison between CCRO and two-stage RO at Y_{tot} = 81%.

	Two-stage RO	CCRO-HPF	CCRO-LPF
Total feed rate (m ³ /h)	346.4	346.4	346.4
Recovery	81 %	81 %	81 %
Feed osmotic pressure (bar)	0.62	0.62	0.62
RO array	$(28:14) \times 7$	294×1	294×1
Number of elements	294	294	294
RO element	BW30-400	BW30-400	BW30-400
Element area (m ²)	37	37	37
Membrane permeability (lmh/bar)	2.79	2.79	2.79
Average flux per element (lmh)	25.7	25.7	25.7 ^a
Filtration time to flushing time	00	37.4:1	42.6:1
Recovery per element	varies	10 %	10 %
Feed per vessel (m ³ /h)	12.4/9.3 ^b	9.5	9.8

^a 26.3 lmh during filtration and 0 during flushing.

Table 3Parameters in CCRO model employing one RO element.

Parameters	Value or expression
a_1	$0.086 Q_0^{0.40}$
n_1	0.40
a_2	$0.0065 Q_0^{1.67}$
n_2	1.67
Pe_D	40

Note: The unit for Q_0 is m^3/h . The calculated pressure drop has a unit of bar and the calculated flux and mass transfer coefficient both have a unit of $(m^3/h)/m^2$ [37].

For cyclic simulations of CCRO, the boundary conditions used in the previous work [37] must be modified. For example, in both CC and flushing modes, the dimensionless transmembrane hydraulic pressure at the RO entrance $\Delta P_0/\pi_0$ (or $\theta(0,t^*)$) is unknown a priori. Instead, it should be determined such that the dimensionless flow rate at the end of the RO meets the process specification (1 – Y_{SP} for HPF and 1 for LPF). Moreover, in the CC mode, the feed to the RO is a mixture of the fresh feed and the recycle stream, whose concentration varies as a function of time ($Y_{SP}C_0+(1-Y_{SP})C(t,L)$). The boundary conditions for different modes in CCRO are summarized in Table 4.

Eq. (6) is discretized by orthogonal collocation following a similar approach presented previously [37]. The boundary conditions in Table 4 are used to describe variables at the boundary points by those at the interior points. As a result, the PDEs are converted to a set of differential-algebraic equations (DAEs), which are solved by Matlab. It is assumed that the RO is filled with the fresh feed initially (i.e. $C = C_0$ everywhere).

Table 4Boundary conditions in CCRO simulations.

Closed-circuit mode	High-pressure flushing mode	Low-pressure flushing mode
$\left.\left(c^* - \frac{1}{Pe_D} \frac{\partial c^*}{\partial x^*}\right)\right _{x^* = 0^+} =$	$\left. \left(c^* - \frac{1}{Pe_D} \frac{\partial c^*}{\partial x^*} \right) \right _{x^* = 0^+} = 1$	$\left. \left(c^* - \frac{1}{Pe_D} \frac{\partial c^*}{\partial x^*} \right) \right _{x^* = 0^+} =$
$\frac{1+rc^*(1,t^*)}{1+r}$ $\frac{\partial c^* }{\partial c^* }$	∂c^*	∂c^*
$\frac{\partial c^*}{\partial x^*}\Big _{x^*=1} = 0$ $q^*(x^*, t^*)\Big _{x^*=0} = 1$	$\frac{\partial c^*}{\partial x^*}\Big _{x^*=1} = 0$ $q^*(x^*, t^*)\Big _{x^*=0} = 1$	$\begin{vmatrix} \frac{\partial c^*}{\partial x^*} _{x^*=1} = 0 \\ q^*(x^*, t^*) _{x^*=0} = 1 \end{vmatrix}$
$q^*(x^*, t^*) _{x^*=1} = 1 - Y_{SP}$ $\theta'(x^*, t^*) _{x^*=0} = -\frac{a_2}{\pi}$	$q^*(x^*, t^*) _{x^*=1} = 1 - Y_{SP}$ $\theta^{'}(x^*, t^*) _{x^*=0} = -\frac{a_2}{\pi}$	$q^*(x^*, t^*) _{x^*=1} = 0$ $\theta'(x^*, t^*) _{x^*=0} = -\frac{a_2}{\pi}$
$\theta'(x^*,t^*) _{x^*=1} = -$	$\theta'(x^*,t^*) _{x^*=1} = -$	$\theta'(x^*,t^*) _{x^*=1} = -\frac{a_2}{\pi_0}$
$\frac{a_2}{\pi_0}(1-Y_{SP})^{n_2}$	$\frac{a_2}{\pi_0} (1 - Y_{SP})^{n_2}$	

3. Results and discussion

3.1. Average flux = 24.5 lmh, recovery = 90 %

The mathematical model (Eq. (6) with boundary conditions shown in Table 4) is solved using design conditions in Table 1 and parameters in Table 3 for 10 filtration and flushing cycles in CCRO-HPF and CCRO-LPF. The flushing time period is set to be one space time (i.e. $t_{FL} = \tau$). For both flushing schemes, it is shown that the CSS can be reached in just a few cycles. This has been confirmed in experimental studies [19].

The spatiotemporal profiles of the dimensionless flow in the 10th cycle are shown in Fig. 2. For both CCRO-HPF and CCRO-LPF, the shapes of Q/Q_0 in the CC mode are similar to a flat paper with wrinkles near the left edge (corresponding to the beginning of the CC mode). This is due to the propagation of the concentration wave (to be shown later) when the operation mode transits from flushing to CC. The shapes of Q/Q_0 in the flushing mode, however, are similar to a net with two flat edges (corresponding to the entrance and outlet of RO). The fact that the flow rate decreases slightly, and then comes back to its original value in LPF implies osmotic drawback near the end of the RO element.

A plot of driving forces at five different progression times $(t_1 - t_5)$ of CC and flushing in the last cycle (shown in Fig. 3) indicates that their spatial average is time-invariant. However, at any moment, there is a spatial variation of driving force, and therefore, local flux. For most of the time, the driving force reduces monotonically along the flow direction. It becomes negative near the end of the membrane during LPF, which confirms reverse flux. It should be noted that the dimensionless driving force during filtration is much greater than zero, implying that the operation is far away from the thermodynamic limit. This is a major difference between brackish and seawater ROs [43].

The spatiotemporal profiles of the dimensionless transmembrane pressure ($\theta = \Delta P/\pi_0$) in the last cycle of the simulation are shown in Fig. 4. All profiles are all similar to a quadrilateral placed in a spatiotemporal coordinate system. Even though a relatively small pressure, which serves to overcome the flow resistance, is needed for LPF, the pressure level in the CC mode of CCRO-LPF is generally higher than the one used in CCRO-HPF in order to maintain the same recovery.

The spatiotemporal profiles of the dimensionless salt concentration $(c^* = C/C_0)$ in the 10th cycle are shown in Fig. 5. In both LPF and HPF, there is a spatial variation of concentration at the end of the flushing cycle (i.e. the salt concentration is approximately C_0 at the RO entrance but much greater at the outlet). When CC is resumed, the interplay between dispersion, convection and permeation causes fluctuations in the salt concentration for a period lasting several space times. The oscillation followed by a linear profile in salt concentration has been confirmed by conductivity measurements [44]. After a sufficient time has elapsed, the dispersion term becomes relatively small. As a result, the driving force decreases monotonically along the axial direction (shown in Fig. 3), and the salt concentration increases steadfastly.

Fig. 6 shows the spatial profiles of concentration at the CSS. They are switched back and forth between cycles. As compared to HPF, LPF reduces the salt concentration to a slightly lower level at the end of the flushing cycle, even though the RO is initially loaded with more salt [37]. However, when the CC mode and flushing mode are coupled for cyclic operation, a higher flux and a longer filtration period are required to maintain the same water production in CCRO-LPF, which in turn, lead to a higher concentration at the end of the CC cycle. In CCRO-LPF, the dimensionless concentrate concentration is greater than 10 (or $1/(1 - Y_{tot})$) at both ends of the RO. In CCRO-HPF, it is above 10 at the outlet but below 10 at the entrance. The wide range of salt concentration levels in CCRO-LPF is consistent with the range of pressure levels shown in Fig. 4.

Fig. 7 shows the temporal profile of concentrate concentration C_c and spatial average concentration $(\overline{C} = \int_0^L C dx/L)$ in 10 cycles. The minima of \overline{C} occur at the end of flushing cycles. The minima of C_c , however,

^b No interstage booster pump.

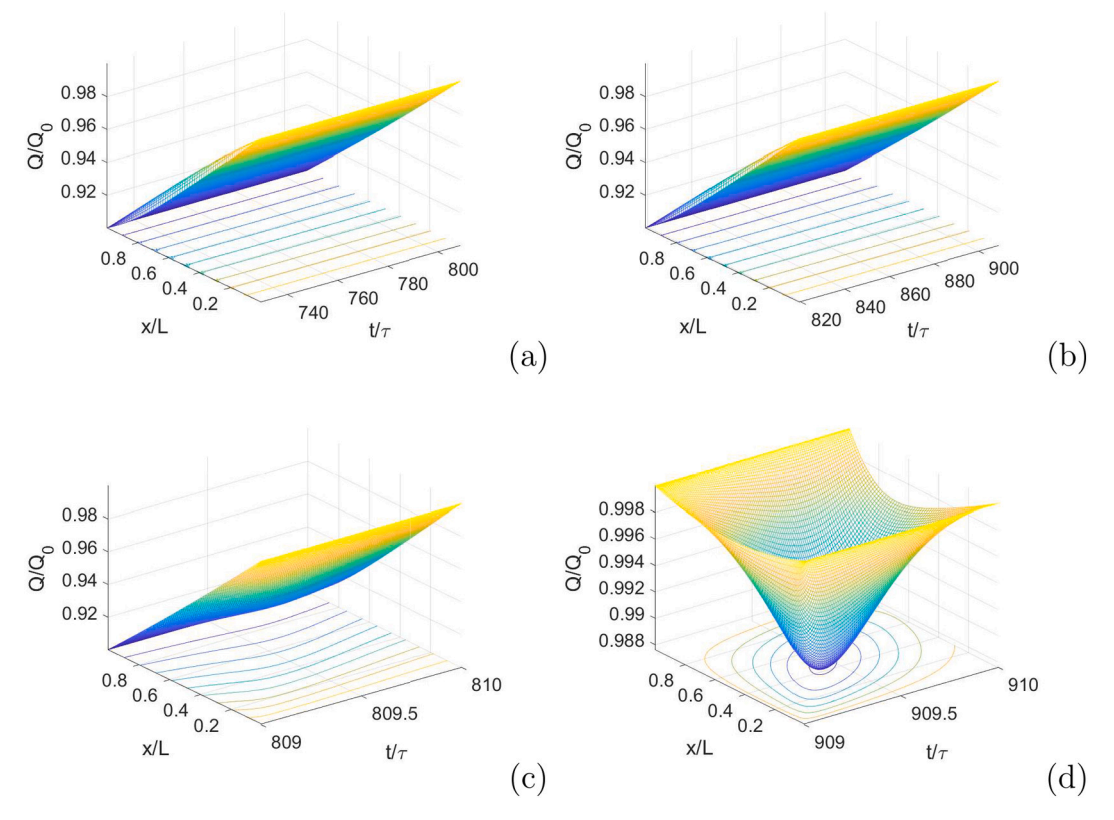


Fig. 2. Spatiotemporal profiles of Q/Q_0 in (a) CC mode of CCRO-HPF, (b) CC mode of CCRO-LPF, (c) flushing mode of CCRO-HPF, and (d) flushing mode of CCRO-LPF.

occur slightly after the beginning of the CC cycles. Because of distribution of residence times in the spacer-filled channel, flushing the circuit with a volume equivalent to V_c cannot completely expel out the brine solution in the RO channel [42]. This has been confirmed by experiments [19].

For CCRO with no flux in the flushing/refilling step, the author introduced the flushing efficacy parameter (f) such that the average concentration at the end of the flushing cycle is a weighted sum of the concentrate concentration and flushing fluid concentration [20]:

$$\overline{c}_{i+1}^* = (1 - f) \left[\frac{Y_{tot}}{1 - Y_{tot}} + \overline{c}_i^* \right] + f \tag{7}$$

where $\overline{c}^* = \overline{C}/C_0$ and i and i+1 represent two consecutive cycles. At the CSS.

$$\overline{c}_{CSS}^* = 1 + \frac{Y_{tot}(1 - f)}{f(1 - Y_{tot})} \tag{8}$$

Eq. (8) with f=0.912 matches the cyclic data very well, as shown in Fig. 7(d). In this case, $\overline{c}_{CSS}^* = 1.87$. These are consistent with the author's previous CFD study which suggested Pe_D =42 and f=0.9 for one BW30-400 RO element [42].

After the results at the CSS are obtained, the SEC normalized by the feed osmotic pressure (NSEC) can be calculated. There are four terms in the energy calculations: (1) pump energy to drive the raw feed in the CC mode, (2) pump energy to recycle the concentrate to the entrance of the RO, (3) pump energy to drive the raw feed in the flushing mode, and (4) energy of the concentrate that may be recovered by an ERD. If the permeate channel is at atmospheric pressure, the theoretical NSEC is calculated as follows:

$$NSEC = \frac{Y_{SP} \int_{0}^{t_{FT}^{*}} \theta(0, t^{*}) dt^{*} + (1 - Y_{SP}) \int_{0}^{t_{FT}^{*}} [\theta(0, t^{*}) - \theta(1, t^{*})] dt^{*}}{Y_{SP} t_{FL}^{*} + \delta Y_{SP} t_{FL}^{*}} \theta(1, t^{*}) dt^{*}}$$

$$(9)$$

Each term in the numerator in Eq. (9) may be modified by the pump efficiency or the ERD efficiency to calculate the actual NSEC.

The inlet pressure is approximately a linear function of time, as shown in Fig. 8. Such a trend was also observed in bench- and pilot-scale experiments [18,19,28]. The initial and final pressures in the CC modes are 10.5 bar and 16.1 bar in CCRO-HPF, and 10.4 bar and 16.7 bar in CCRO-LPF. The CCRO-LPF does start with a slightly lower pressure in CC mode, but eventually ends with a higher pressure in comparison to CCRO-HPF. The initial and final pressures in the flushing modes are 16.1 bar and 10.5 bar in CCRO-HPF, and 6.9 bar and 1.3 bar in CCRO-LPF. The pressure drop across the CCRO element in each operation mode is fairly constant because the flow profile barely changes. For CC-HPF, it is 0.24 bar in both CC and flushing modes. For CC-LPF, it is 0.244 bar in CC and 0.265 bar in flushing. The constant pressure drops were observed in pilot experiments [28].

In addition to the baseline case based on parameters from Table 3, parametric analysis is also carried out to study the effect of flow resistance, concentration polarization and axial dispersion on energy performance. For example, increasing a_1 by 100 times will essentially eliminate the effect of concentration polarization. Similarly, reducing a_2 by 100 fold will largely remove the effect of flow resistance. Increasing Pe_D by 25 times may suppress the effect of dispersion to some extent because there may be "numerical dispersion" – a computational artifact, at high Peclet numbers.

The results are summarized in Table 5. The effects of pressure drop, mass transfer and axial dispersion on energy consumption are

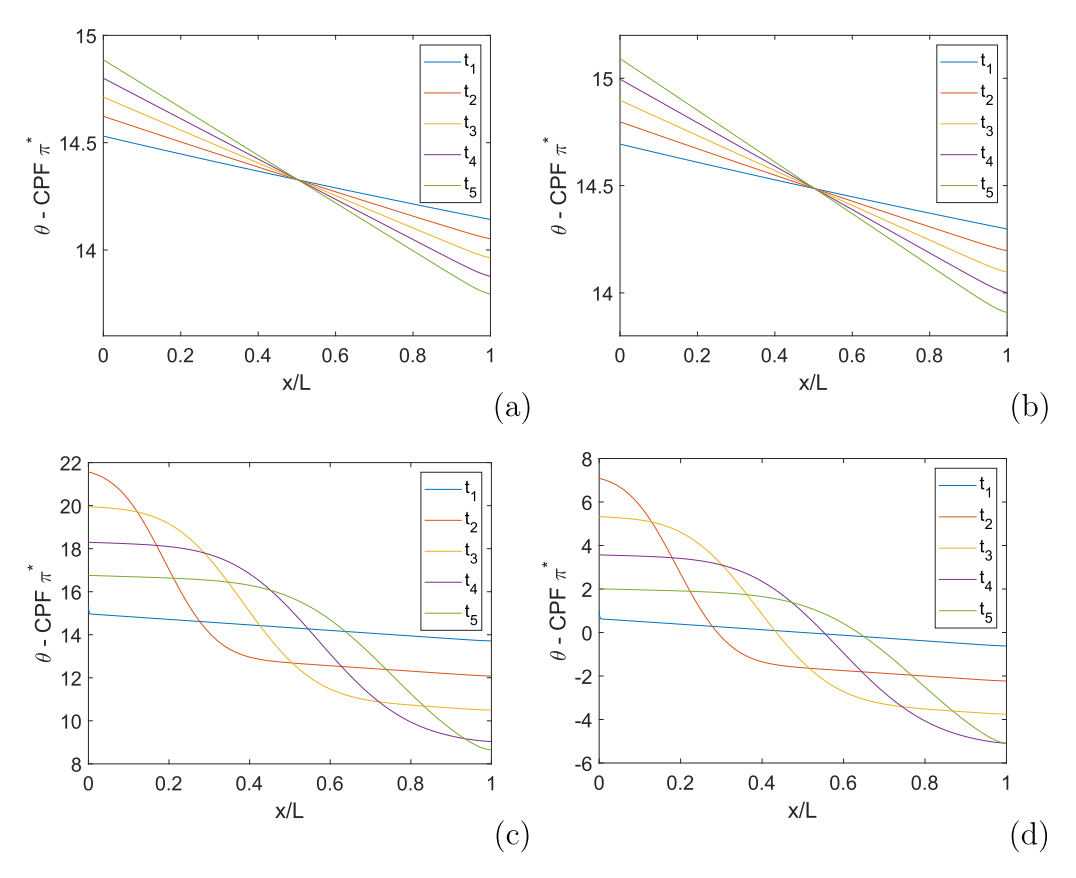


Fig. 3. Dimensionless driving force $((\Delta P - CPF \cdot \pi)/\pi_0)$ in (a) CC mode of CCRO-HPF, (b) CC mode of CCRO-LPF, (c) flushing mode of CCRO-HPF, and (d) flushing mode of CCRO-LPF.

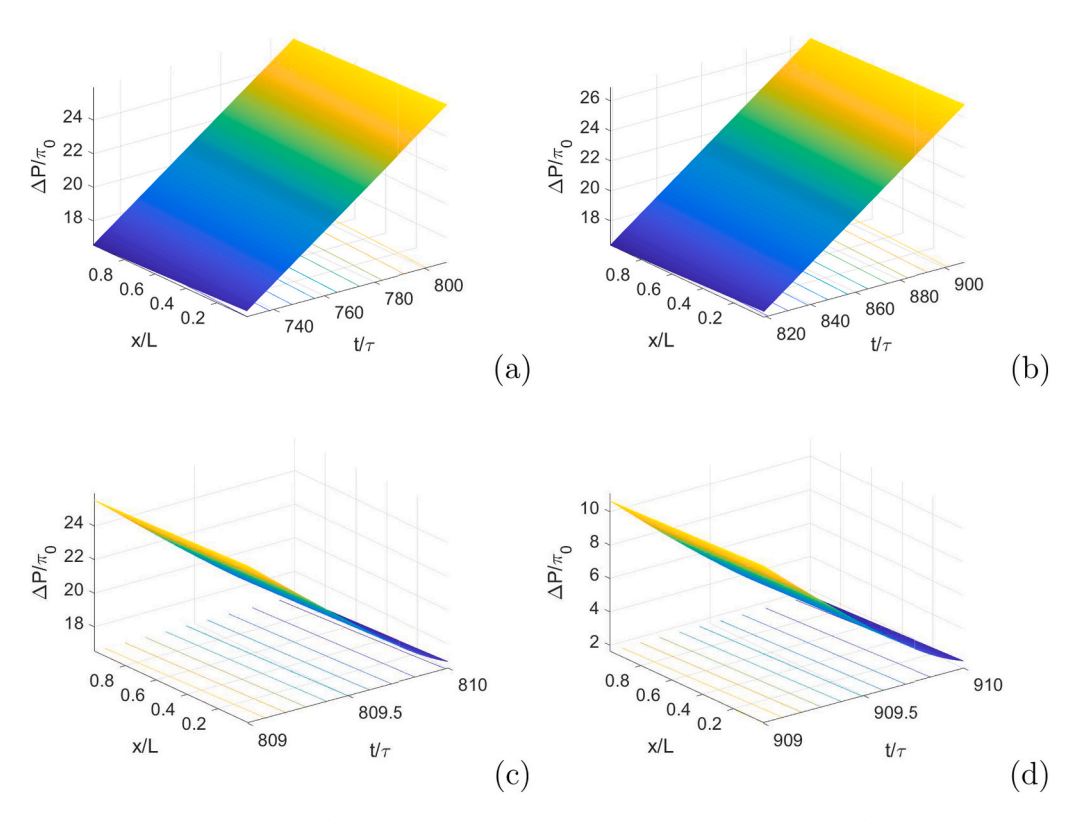


Fig. 4. Spatiotemporal profiles of $\Delta P/\pi_0$ in (a) CC mode of CCRO-HPF, (b) CC mode of CCRO-LPF, (c) flushing mode of CCRO-HPF, and (d) flushing mode of CCRO-LPF.

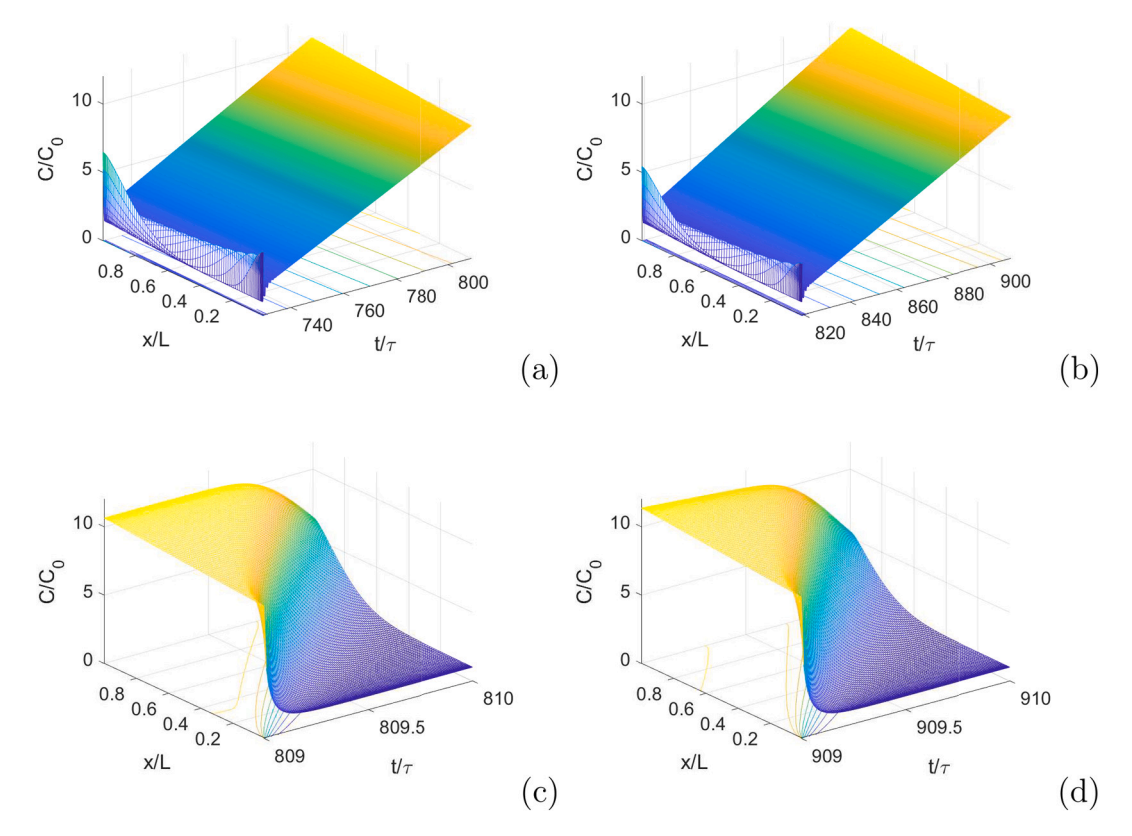


Fig. 5. Spatiotemporal profiles of C/C_0 in (a) CC mode of CCRO-HPF, (b) CC mode of CCRO-LPF, (c) flushing mode of CCRO-HPF, and (d) flushing mode of CCRO-LPF.

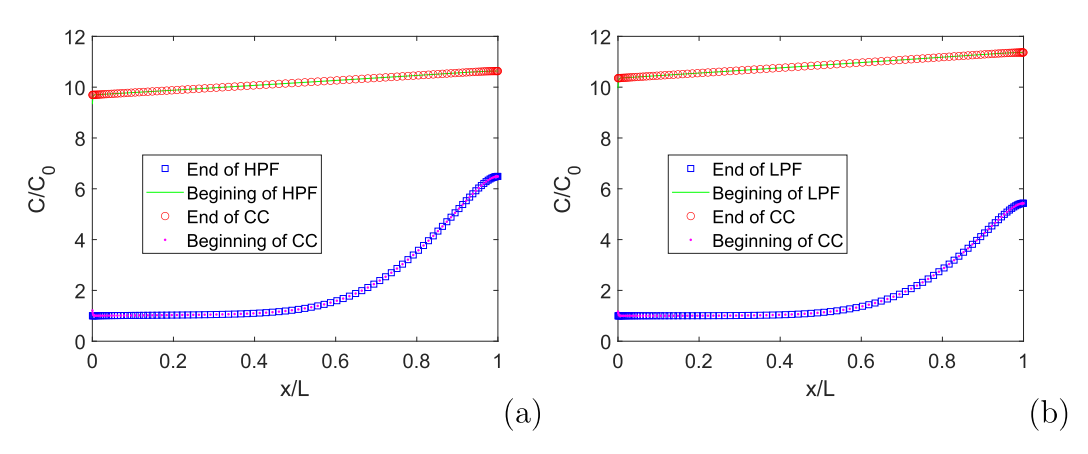


Fig. 6. Spatial profiles of C/C_0 at CSS in (a) CCRO-HPF and (b) CCRO-LPF.

approximately additive. For CCRO-LPF, the author derived an analytical expression for NSEC if the effect of pressure drop and concentration polarization are not taken into consideration [20]. Specifically, the contribution of flux to NSEC is:

$$\frac{Y_{tot}}{\gamma_{LPF}} = \frac{\overline{J}_{w,FT}}{L_p \pi_0} \tag{10}$$

where $\gamma_{LPF}=\frac{A_mL_p\pi_0}{(Q_0Y_{SPtpr}+Q_0t_{PL})/t_{FT}}$ for LPF. In this particular case, Y_{tot} =0.9, γ_{SBRO} =0.0621, $\overline{J}_{W,FT}=$ 24.8 lmh. An evaluation of either side of Eq. (10) yields 14.49. The NSEC imposed by thermodynamics is 1 + Y_{tot} /[2(1 - Y_{tot})]=5.50. The NSEC due to salt retention is $\frac{Y_{tot}(1-f)}{f(1-Y_{tot})}=$ 0.87. It is seen that the sum of all three terms (20.9) matches exactly with the value of case 5 in Table 5. Therefore, it is determined that the contributions of

flux, thermodynamic restriction, flow resistance, concentration polarization and salt retention are 14.49, 5.50, 3.84, 0.75 and 0.87, respectively. The sum (25.4) is in perfect consistency with the result in the baseline case. For CCRO-HPF, an analytic solution to NSECs due to finite flux, thermodynamic restriction and flushing efficacy is not yet available. If the same analytical formulas from CCRO-LPF are used for estimation, the total NSEC (25.1=14.33 + 5.50 + 3.64 + 0.72 + 0.87) is only 0.6 % higher than the result shown in case 1. Note that NSEC imposed by finite flux in CCRO-HPF is 14.33 (instead of 14.49) because the average flux in filtration is slightly smaller (24.5 lmh) than the one in CCRO-LRF (24.8 lmh).

The contributing factors to NSEC in both CCROs can be described by the pie chart in Fig. 9 with an error margin of 1 %. It is clear that the flux requirement accounts for a major portion of the energy consumption,

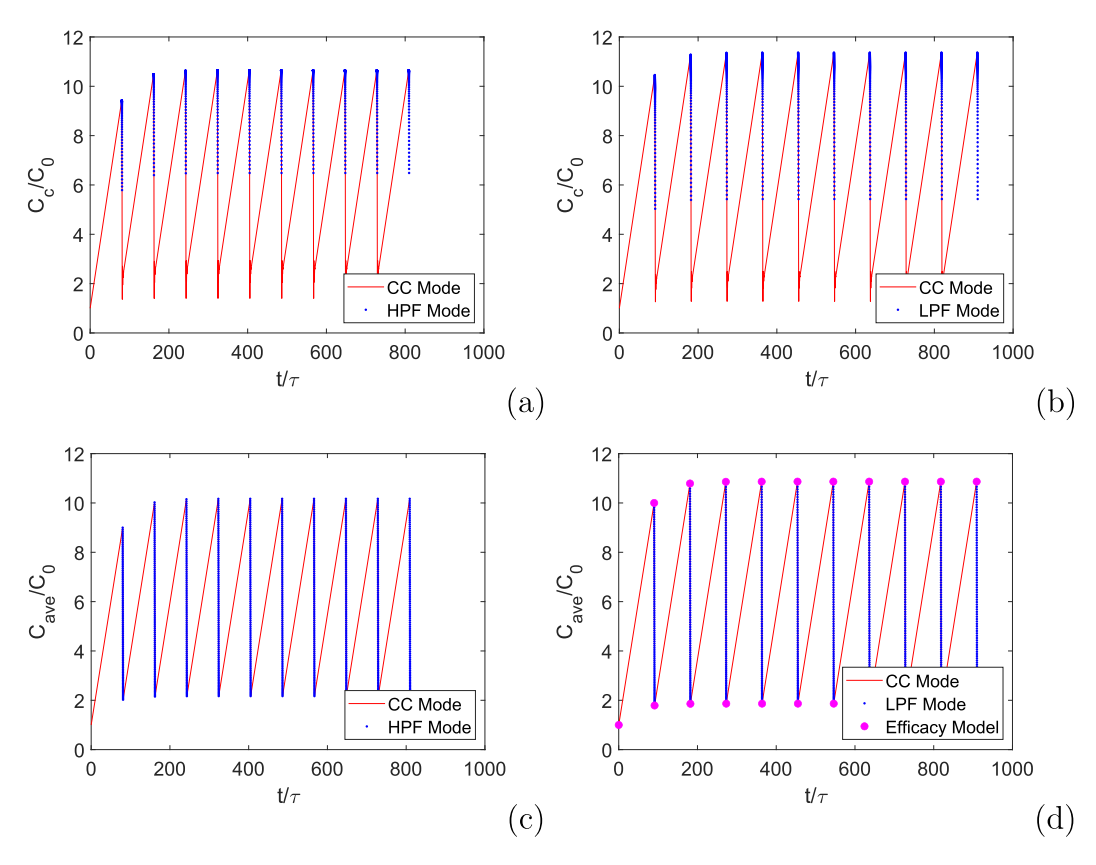


Fig. 7. Temporal profiles of (a) C_c/C_0 in CCRO-HPF, (b) C_c/C_0 in CCRO-LPF, (c) spatial average C/C_0 in CCRO-HPF, (d) spatial average C/C_0 in CCRO-LPF.

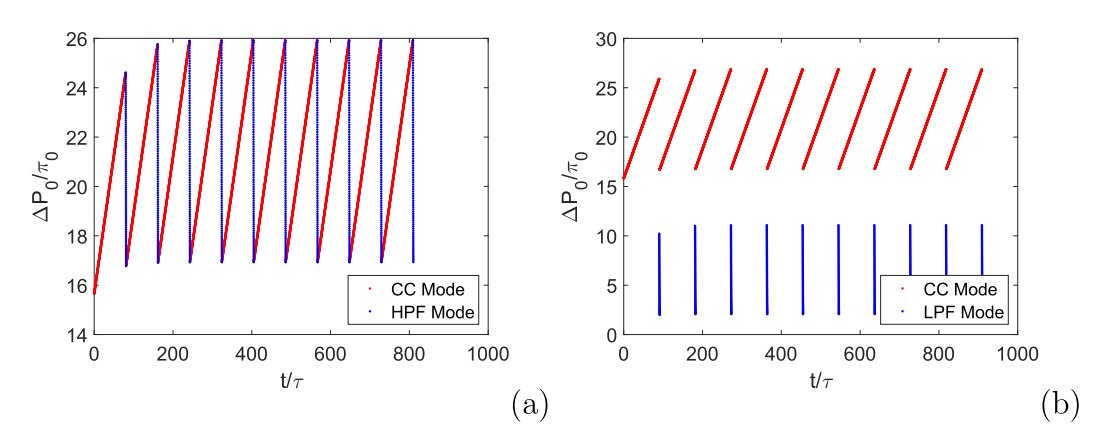


Fig. 8. Temporal profiles of $\Delta P_0/\pi_0$ in (a) CCRO-HPF and (b) CCRO-LPF.

due to the fact that the process is operated far from the thermodynamic limit (see Fig. 3).

The NSECs for CCRO-HPF and CCRO-LPF at 90 % recovery and 24.5 lmh flux are 24.9 and 25.4 with ERD (or 27.2 and 26.1 without ERD). For steady-state three-stage RO without booster pumps or ERDs under the same conditions shown in Table 1, $\Delta P_0/\pi_0$ at the beginning of the first stage, which is essentially the theoretical NSEC in this particular case, is only 20.6 [34]. It is noted that most high-recovery BWRO plants do not have ERDs because the relatively low brine flow and pressure (as compared to those in SWRO) may not justify installation [45]. If two booster pumps are installed to improve flux uniformity in this three-stage design, the NSEC increases by about 0.5 % [34].

The energy performance of CCRO, with either HPF or LPF, does not compare favorably to state-of-the-art multi-stage designs for such a low-

salinity brackish water RO. In several papers [5,8,43], the author has shown that staged operations with booster pumps and batch operations with internal staging features are energy advantageous only if γ is sufficiently large and friction loss is insignificant, where thermodynamic restriction is the dominant factor for NSEC. In such a case, gradually increasing the hydraulic pressure significantly enhances flux uniformity, resulting in a reduction in the NSEC [5]. When γ is small, the operation is far from the thermodynamic limit (or the transmembrane pressure sits way above the osmotic pressure; it mainly serves to satisfy the flux requirement and to overcome the friction loss), the benefit of an everincreasing hydraulic pressure profile is minimal from a viewpoint of energy efficiency. As a comparison, γ is about 1 in SWRO plants and only 0.06 in this BWRO case study. Moreover, CCRO is associated with undesired entropy generation due to the mixing of the fresh feed and the

Table 5 Analysis of NSEC in CCROs with high- and low-pressure flushing. $\bar{J}_w = 24.5$ lmh, $Y_{tot} = 90\%$, $\pi_0 = 0.62$ bar.

Case	CCRO w	ith HPF					CCRO w	rith LPF				
	CC	Flushing	Recycle	ERD	Net	Difference	CC	Flushing	Recycle	ERD	Net	Difference
1	21.2	2.6	3.4	-2.3	24.9		21.8	0.7	3.5	-0.7	25.4	
2	20.4	2.6	3.4	-2.3	24.2	0.7	21.1	0.7	3.5	-0.7	24.7	0.8
3	21.0	2.6	0.0	-2.4	21.3	3.6	21.6	0.7	0.0	-0.7	21.7	3.8
4	20.5	2.6	3.4	-2.3	24.3	0.6	21.1	0.7	3.5	-0.6	24.7	0.7
5	20.3	2.5	0.0	-2.3	20.5	4.4	20.9	0.7	0.0	-0.7	20.9	4.5
6	19.7	2.5	0.0	-2.2	20.0	4.9	20.2	0.6	0.0	-0.6	20.2	5.2

Case 1: Baseline case.

Case 2: The mass transfer parameter (a_1) is enhanced by 100 times.

Case 3: The pressure drop parameter (a_2) is reduced 100 fold.

Case 4: The Peclet number (Pe_D) is enhanced by 25 times.

Case 5: Both parameters for mass transfer and pressure drop are varied.

Case 6: All the three parameters are varied simultaneously.

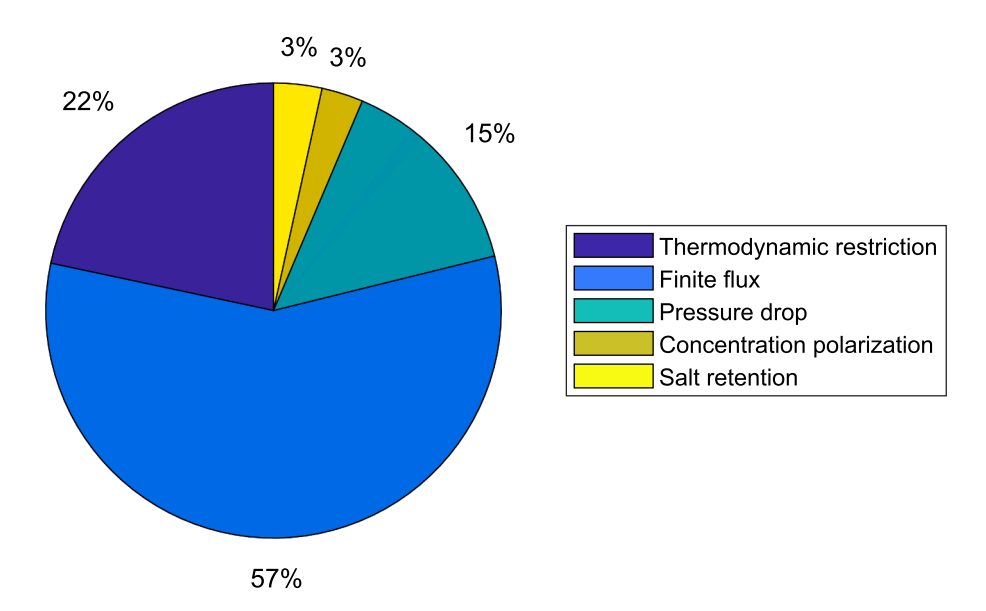


Fig. 9. Contributing factors to SEC in CCRO. Feed osmotic pressure: 0.62 bar. Average flux: 24.5 lmh. Recovery: 90 %.

recycled stream, which have drastically different concentrations. This adversely affects its energy performance.

From Fig. 9 and the analytical solution published previously [20], the most effective way to reduce NSEC in CCRO is to reduce Q_0 or \overline{J}_w . A smaller Q_0 implies a larger γ and a reduced pressure drop, both will save energy consumption. The effect of Q_0 on NSEC determined by the mathematical model is shown in Fig. 10. Halving Q_0 will bring NSEC to a value about 16. However, one drawback is that the number of RO elements may be doubled to maintain the same water production. Another potential issue is that the cross velocity may not satisfy the minimum requirement recommended by membrane manufacturers.

One may conjecture that extending the flushing time period in CCRO may help reduce salt buildup and therefore, energy consumption. This supposition is not supported by the simulation results shown in Fig. 11. Doubling the flushing time period does lower the concentration to the minimum level at the end of the flushing cycle. However, the concentration at the end of the CC cycle is elevated because of a prolonged CC step. As a consequence, the applied pressure varies in a wider range and its time-average is higher. Several flushing periods are tried in the simulation and their corresponding energy consumptions are summarized in Fig. 13. It appears that a flushing period lasting one space time is the most energy efficient. These are in general agreement with pilot-scale experimental studies conducted by Cohen and coworkers [19]. Results presented in this work, unless stated specifically, are based on the optimal flushing time.

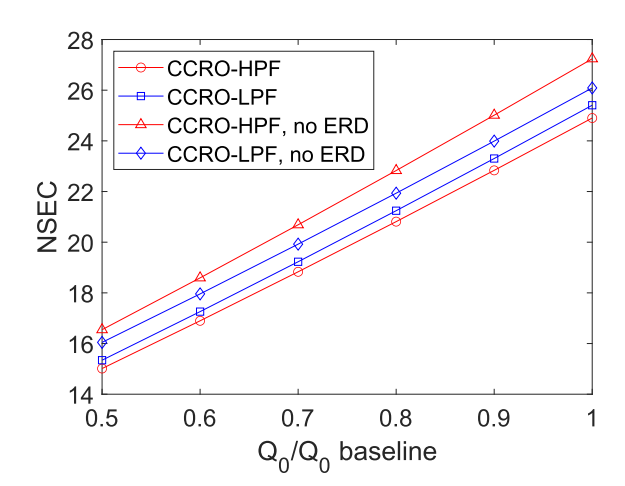


Fig. 10. Effect of Q_0 on NSEC. Feed osmotic pressure: 0.62 bar. Average flux: 24.5 lmh. Recovery: 90 %. Baseline Q_0 is 9.1 m³/h for CCRO-HPF and 9.2 m³/h for CCRO-LPF.

To reduce capital expenditure (CapEx) in CCRO, it is common to enclose multiple elements in each pressure vessel, which allows a larger single pass recovery rate. A general rule of thumb is that $Y_{SP}=1-(1-0.1)^{N_E}$, where N_E is number of elements per vessel. As N_E increases, the

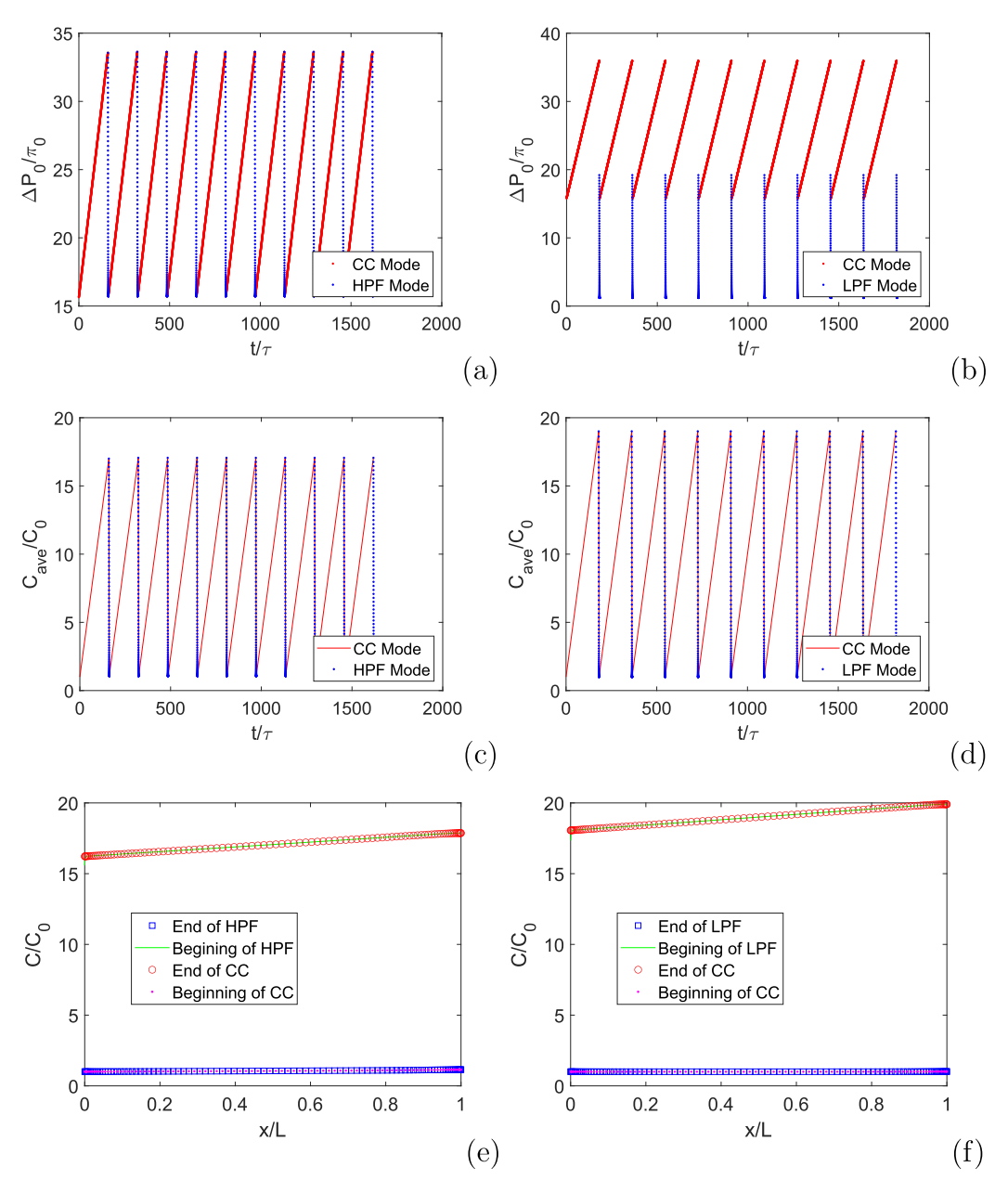


Fig. 11. Effect of doubling flushing time on (a, b) pressure, (c, d) spatial-average concentration and (e, f) spatial concentration profile at CSS in CCRO.

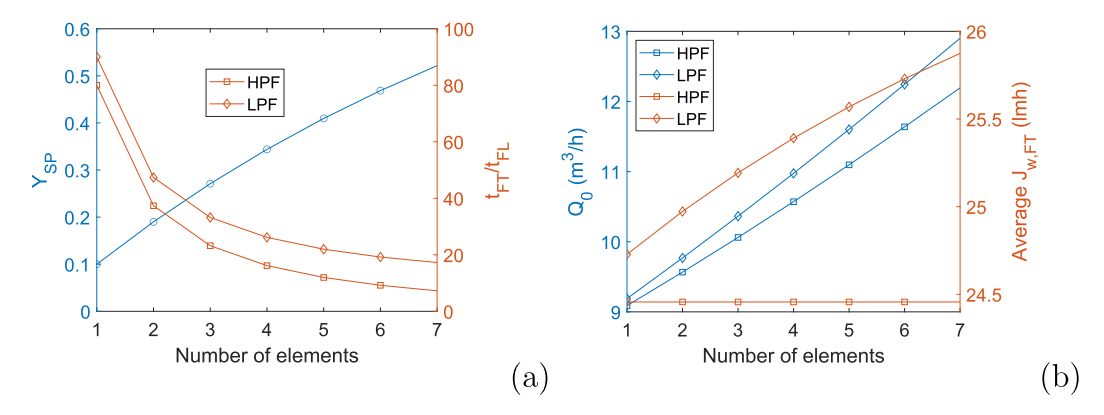


Fig. 12. Effect of number of elements per vessel on (a) Y_{SP} and t_{FT}/t_{FL} and (b) Q_0 and $\overline{J}_{W,FT}$.

 t_{FT}/t_{FL} will decrease while Q_0 will increase in both HPF and LPF, as shown in Fig. 12. N_E is changed to 3 (or 114 vessels) and 7 (or 49 vessels) to maintain roughly the total number of RO elements (343). Larger values of Pe_D (45 if N_e =3 and 50 if N_e =7) are used to reflect the fact that the spacer-filled channel is closer to a plug flow reactor as the number of elements increases [42]. The results are shown in Table 6. For CCRO-HPF, the NSEC remains nearly identical (24.7 and 24.8 respectively with ERD and 26.9 and 26.9 without ERD). For CCRO-LPF, the NSEC increases as N_E increases (26.0 and 27.2 respectively with ERD and 26.6 and 27.6 without ERD), because of a larger flux in the CC mode (Fig. 12 (b)).

3.2. Average flux = 25.7 lmh, recovery = 81 %

The model is solved again using design conditions shown in Table 2 for 10 filtration and flushing cycles. The results of pressures, concentrations, and flow rates follow similar trends to these presented in Section 3.1. Parametric analysis is conducted to study the effect of concentration polarization, flow resistance and flushing efficacy on energy consumption. The numerical results are summarized in Table 7.

It is validated that the same flushing efficacy model (Eq. (7)) with f=0.912 predicts the cycle-to-cycle spatial average concentration data very well, similar to Fig. 7(d). For CCRO-LPF, the NSEC penalized by imperfect flushing is $\frac{Y_{tot}(1-f)}{f(1-Y_{tot})} = 0.41$. It is determined that the contributions of flux, thermodynamic restriction, flow resistance, concentration polarization and salt retention are 15.40, 3.13, 4.21, 0.44, and 0.41, respectively.

The pie chart describing relative contributions of thermodynamics, finite flux, flow resistance, concentration polarization and imperfect flushing to NSEC is shown in Fig. 14. It is observed that the percentage of finite flux is even higher than that in Fig. 9 because of a larger design flux. The friction loss causes more energy than the thermodynamic restriction. An examination of pressure drops in the CC mode and LPF mode indicates that they are at higher levels (0.27 bar and 0.29 bar) than those in Section 3.1. The higher pressure drops are associated with a larger Q_0 (9.8 m³/h in CCRO-LPF) used in the two-stage design.

The NSECs for CCRO-HPF and CCRO-LPF at 81 % recovery and 25.7 lmh are 22.9 and 23.6 with ERD (or 27.3 and 24.4 without ERD). For a two-stage RO without booster pump or ERD under the same flow and recovery conditions shown in Table 2, $\Delta P_0/\pi_0$ (or the theoretical NSEC) at the beginning of the first stage is only 20.0 based on both plant measurements and model predictions [41]. This further shows that CCRO is not as energy-efficient as state-of-the-art multi-stage designs for low-salinity brackish water desalination.

4. Concluding remarks

A spatiotemporal model is presented for the first time for cyclic simulations of CCRO. The model couples the CC mode and the flushing mode and allows detailed studies of design and operating conditions on process performance at the CSS. The computational framework is expected to facilitate experimental studies currently being pursued in many research groups and desalination facilities.

The potential energy benefit of CCRO relative to conventional multistage RO suggested in literature is not supported by this study. For brackish water desalination, the membrane capacity to intake ratio (or

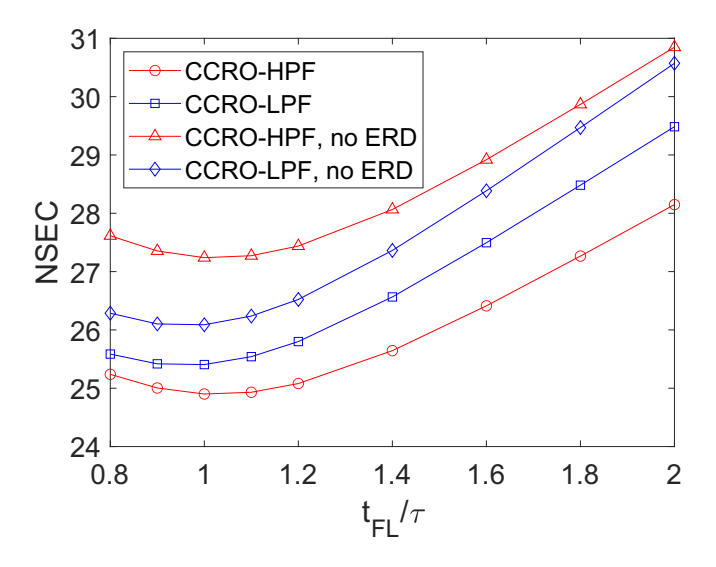


Fig. 13. Effect of flushing time on NSEC. Feed osmotic pressure: 0.62 bar. Average flux: 24.5 lmh. Feed osmotic pressure: 0.62 bar. Average flux: 24.5 lmh.

the γ parameter) is too small to allow internal staging to prevail. In such a case, the most dominant factor to NSEC is the design flux. The friction loss also accounts for a fair portion of the energy requirement. These are different from the case of SWRO in which thermodynamic restriction is the major contributing factor to NSEC. For SWRO applications, CCRO is likely to be plagued by salt retention and the highest allowable pressure for the membrane. It is suspected that CCRO is positioned for treatment of water with moderate high salinities, though detailed studies are required to confirm it.

When the CC mode and the flushing mode are coupled in cyclic operations, high pressure flushing will help maintain concentrations and pressures at relatively lower levels. The SEC is also slightly lower if the concentrate energy is recovered. However, without energy recovery, CCRO with low pressure flushing is more energy efficient.

As the number of elements per vessel increases, a larger single pass recovery may be adopted in process design. The pressure vessel is longer, and the recycle to fresh feed ratio (*r*) is smaller. The number of elements per vessel barely affects the energy performance of CCRO-HPF. However, as more elements are enclosed per vessel, the NSEC in CCRO-LPF becomes higher, because it necessitates a higher average flux in the CC mode.

As compared to state-of-the-art multi-stage designs, CCRO has relatively constant flows and recoveries per element. Periodic flushing of membrane may mitigate fouling to some extent. Operational flexibility is a great advantage of CCRO where recovery is controlled by the CC/flushing time ratio. However, the rear-end of the membrane at the end of the CC cycle, even under optimal conditions, experiences a higher concentration than the one in conventional RO under the same flow and recovery conditions. Once the flushing time period exceeds one space time, the concentration level in the CC mode will go even higher, elevating the risk of scaling. Moreover, the applied pressure in the CCRO varies in a wide range. For a fair amount of time, it is higher than the one in the steady-state counterparts.

Table 6 Effect of number of elements per vessel (N_E) on NSEC in CCRO. $\bar{J}_w=24.5$ lmh, $Y_{tot}=90\%$, $\pi_0=0.62$ bar.

$N_E(Y_{SP})$	CCRO with HPF					CCRO w	CCRO with LPF					
	CC	Flushing	Recycle	ERD	Net	Net (no ERD)	CC	Flushing	Recycle	ERD	Net	Net (no ERD)
1 (10 %)	21.2	2.6	3.4	-2.3	24.9	27.2	21.8	0.7	3.5	-0.7	25.4	26.1
3 (19 %)	20.6	3.3	3.0	-2.3	24.7	26.9	22.5	0.8	3.3	-0.6	26.0	26.6
7 (27 %)	19.5	5.2	2.3	-2.2	24.8	26.9	23.8	1.0	2.8	-0.4	27.2	27.6

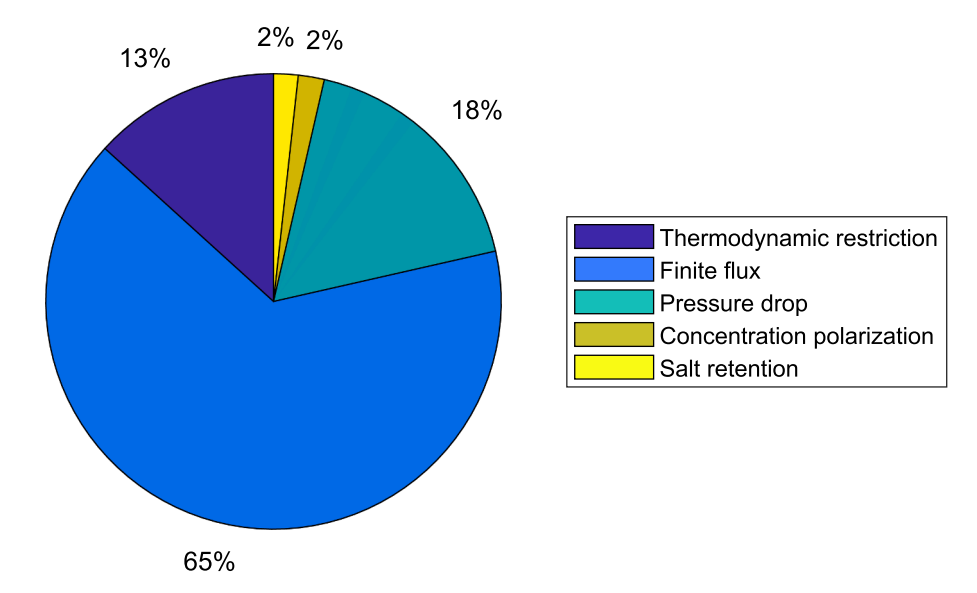


Fig. 14. Contributing factors to SEC in CCRO. Feed osmotic pressure: 0.62 bar. Average flux: 25.7 lmh. Recovery: 81 %.

Table 7 Analysis of NSEC in CCROs with high- and low-pressure flushing. $\bar{J}_w = 25.7$ lmh, $Y_{tot} = 81\%$, $\pi_0 = 0.62$ bar.

Case	CCRO w	rith HPF					CCRO w	rith LPF							
	CC	Flushing	Recycle	ERD	Net	Difference	CC	Flushing	Recycle	ERD	Net	Difference			
1	18.6	5.0	3.7	-4.4	22.9		19.6	0.9	3.9	-0.8	23.6				
2	18.2	4.9	3.7	-4.3	22.5	0.4	19.2	0.9	3.9	-0.8	23.2	0.4			
3	18.4	4.9	0.0	-4.4	18.9	3.9	19.4	0.8	0.0	-0.8	19.4	4.2			
4	18.3	4.9	3.7	-4.3	22.6	0.3	19.2	0.8	3.9	-0.7	23.3	0.4			
5	18.0	4.8	0.0	-4.3	18.5	4.4	18.9	0.8	0.0	-0.8	19.0	4.7			
6	17.7	4.7	0.0	-4.3	18.2	4.6	18.6	0.8	0.0	-0.8	18.7	5.0			

Case 1: Baseline case.

Case 2: The mass transfer parameter (a_1) is enhanced by 100 times.

Case 3: The pressure drop parameter (a_2) is reduced 100 fold.

Case 4: The Peclet number (Pe_D) is enhanced by 25 times.

Case 5: Both parameters for mass transfer and pressure drop are varied.

Case 6: All the three parameters are varied simultaneously.

Flow reversal and retentate recycle (FRRR) with a time-varying ratio has been proposed ultra-high recovery BWRO [34]. It is based on the conventional multi-stage design with dynamic and cyclic characteristics added on it. Different from CCRO, the retentate recycle is introduced only near the end of the course and is activated on an as-needed basis. It is shown by design simulations that FRRR has a lower SEC and a lower concentration level than those in CCRO under similar conditions.

concentration level than the
Nomenclature

BWRO	Brackish water reverse osmosis
CCRO	Closed-circuit reverse osmosis
CPF	Concentration polarization factor
CSS	Cyclic steady state
DAE	Differential algebraic equation
ERD	Energy recovery device
FRRR	Flow reversal with retentate recycle
HPF	High pressure flushing
LPF	Low pressure flushing
NSEC	Normalized specific energy consumption
PDE	Partial differential equation
PFRO	Pulse flow reverse osmosis
RO	Reverse osmosis
SEC	Specific energy consumption
SWRO	Seawater reverse osmosis

ΔP	Transmembrane hydraulic pressure
δ	0 for LPF and 1 for HPF
γ	Membrane capacity intake ratio
π	Osmotic pressure
τ	Space time
θ	Transmembrane pressure divided by feed osmotic pressure
A_m	Membrane area
C	Salt concentration
c*	Dimensionless salt concentration
f	Flushing efficacy
J_w	Water flux across membrane
k_m	Mass transfer coefficient
L	Total length of a pressure vessel
L_p	Hydraulic permeability
$\dot{Pe_D}$	Dispersive Peclet number

Time

Length

Volumetric flow rate

Dimensionless time

Volume of the circuit

Recycle to fresh feed ratio

Dimensionless volumetric flow rate

Q

 q^*

t

 V_c

x

ave	Average
c	Concentrate
FL	Flushing
FT	Filtration
i	Index
p	Permeate
tot	Tot

CRediT authorship contribution statement

Mingheng Li: Conceptualization, Methodology, Software, Writing – original draft, Writing – review & editing, Visualization, Funding acquisition.

Declaration of competing interest

The author declares that there are no known competing financial interests or personal relationships that could have appeared to influence the work reported in this paper.

Data availability

Data will be made available on request.

Acknowledgements

The author would like to acknowledge financial support from the National Science Foundation (CBET-2140946). Any opinions, findings, and conclusions or recommendations expressed in this material are those of the author and do not necessarily reflect the views of the National Science Foundation.

References

- [1] J. Kucera, Desalination: Water From Water, John Wiley & Sons, 2019.
- [2] S. Burn, S. Gray, Efficient Desalination by Reverse Osmosis: A Guide to RO Practice, IWA Publishing London, UK, 2016.
- [3] M. Li, Analysis And Design of Membrane Processes: A Systems Approach, AIP Publishing, Melville, New York, November 2020.
- [4] E. Jones, M. Qadir, M.T.H. van Vliet, V. Smakhtin, S. Kang, The state of desalination and brine production: a global outlook, Sci. Total Environ. 657 (2019) 1343–1356.
- [5] M. Li, Dynamic operation of batch reverse osmosis and batch pressure retarded osmosis, Ind. Eng. Chem. Res. 59 (2020) 3097–3108.
- [6] A. Zhu, P.D. Christofides, Y. Cohen, Effect of thermodynamic restriction on energy cost optimization of RO membrane water desalination, Ind. Eng. Chem. Res. 48 (2009) 6010–6021.
- [7] R.L. Stover, Seawater reverse osmosis with isobaric energy recovery devices, Desalination 203 (2007) 168–175.
- [8] M. Li, Minimization of energy in reverse osmosis water desalination using constrained nonlinear optimization, Ind. Eng. Chem. Res. 49 (2010) 1822–1831.
- [9] J. Rioyo, V. Aravinthan, J. Bundschuh, M. Lynch, A review of strategies for RO brine minimization in inland desalination plants, Desalin. Water Treat. 90 (2017) 110–123.
- [10] M. Kurihara, H. Yamamura, T. Nakanishi, S. Jinno, Operation and reliability of very high-recovery seawater desalination technologies by brine conversion twostage RO desalination system, Desalination 138 (2001) 191–199.
- [11] M. Taniguchi, M. Kurihara, S. Kimura, Behavior of a reverse osmosis plant adopting a brine conversion two-stage process and its computer simulation, J. Membr. Sci. 183 (2001) 249–257.
- [12] N. Kishizawa, K. Tsuzuki, M. Hayatsu, Low pressure multi-stage RO system developed in "mega-ton water system" for large-scaled SWRO plant, Desalination 368 (2015) 81–88.
- [13] A. Efraty . Apparatus for continuous closed circuit desalination under variable pressure with a single container, December 8 2009. US Patent 7,628,921.
- [14] A. Efraty, J. Septon, Closed circuit desalination series no-5: high recovery, reduced fouling and low energy nitrate decontamination by a cost-effective BWRO-CCD method, Desalin. Water Treat. 49 (2012) 384–389.
- [15] R.L. Stover, Industrial and brackish water treatment with closed circuit reverse osmosis, Desalin. Water Treat. 51 (2013) 1124–1130.
- [16] S. Lin, M. Elimelech, Staged reverse osmosis operation: configurations, energy efficiency, and application potential, Desalination 366 (2015) 9–14.

- [17] J.R. Werber, A. Deshmukh, M. Elimelech, Can batch or semi-batch processes save energy in reverse-osmosis desalination? Desalination 402 (2017) 109–122.
- [18] S.M. Riley, D.C. Ahoor, K. Oetjen, T.Y. Cath, Closed circuit desalination of O&G produced water: an evaluation of NF/RO performance and integrity, Desalination 442 (2018) 51–61.
- [19] T. Lee, A. Rahardianto, Y. Cohen, Multi-cycle operation of semi-batch reverse osmosis (SBRO) desalination, J. Membr. Sci. 588 (2019), 117090.
- [20] M. Li, Effects of finite flux and flushing efficacy on specific energy consumption in semi-batch and batch reverse osmosis processes, Desalination 496 (2020), 114646.
- [21] E. Hosseinipour, K. Park, L. Burlace, T. Naughton, P.A. Davies, A free-piston batch reverse osmosis (RO) system for brackish water desalination: experimental study and model validation, Desalination 527 (2022), 115524.
- [22] D.M. Warsinger, E.W. Tow, K.G. Nayar, L.A. Maswadeh, J.H. Lienhard V, Energy efficiency of batch and semi-batch (CCRO) reverse osmosis desalination, Water Res. 106 (2016) 272–282.
- [23] E.M.V. Hoek, A.S. Kim, M. Elimelech, Influence of crossflow membrane filter geometry and shear rate on colloidal fouling in reverse osmosis and nanofiltration separations, Environ. Eng. Sci. 19 (2002) 357–372.
- [24] P. Sanciolo, N. Milne, K. Taylor, M. Mullet, S. Gray, Silica scale mitigation for high recovery reverse osmosis of groundwater for a mining process, Desalination 340 (2014) 49–58.
- [25] A. Antony, J.H. Low, S. Gray, A.E. Childress, P. Le-Clech, G. Leslie, Scale formation and control in high pressure membrane water treatment systems: a review, J. Membr. Sci. 383 (2011) 1–16.
- [26] B. Mansell, P. Ackman, C. Tang, P. Friess, Pilot-scale evaluation of the closed-circuit desalination process for minimizing RO concentrate disposal volume, in: Proceedings of the 30th Annual WateReuse Symposium [CD-ROM], 2015, pp. 13–16.
- [27] A. Waite, W. Broley, M. Ingalsbe, S. Wang, B. Trussell, Can closed circuit desalination boost brackish groundwater and recycled water recovery by squeezing concentrate?, in: AWWA California-Nevada Section Annual Fall Conference, Rancho Mirage, CA, 2018.
- [28] H. Gu, M.H. Plumlee, M. Boyd, M. Hwang, J.C. Lozier, Operational optimization of closed-circuit reverse osmosis (CCRO) pilot to recover concentrate at an advanced water purification facility for potable reuse, Desalination 518 (2021), 115300.
- [29] G. Lauer . Conditioning process and device for producing pure water, November 25 1997. US Patent 5,690,829.
- [30] N. Pomerantz, Y. Ladizhansky, E. Korin, M. Waisman, N. Daltrophe, J. Gilron, Prevention of scaling of reverse osmosis membranes by "zeroing" the elapsed nucleation time. Part I. calcium sulfate, Ind. Eng. Chem. Res. 45 (2006) 2008–2016.
- [31] J. Gilron, M. Waisman, N. Daltrophe, N. Pomerantz, M. Milman, I. Ladizhansky, E. Korin, Prevention of precipitation fouling in NF/RO by reverse flow operation, Desalination 199 (2006) 29–30.
- [32] A.R. Bartman, C.W. McFall, P.D. Christofides, Y. Cohen, Model-predictive control of feed flow reversal in a reverse osmosis desalination process, J. Proc. Contr. 19 (2009) 433–442.
- [33] H. Gu, A.R. Bartman, M. Uchymiak, P.D. Christofides, Y. Cohen, Self-adaptive feed flow reversal operation of reverse osmosis desalination, Desalination 308 (2013) 63–72.
- [34] M. Li, N. Chan, J. Li, Novel dynamic and cyclic designs for ultra-high recovery waste and brackish water RO desalination, Chem. Eng. Res. Des. 179 (2022) 473–483.
- [35] J. Landers, Southern California city seeks to end reliance on imported water. https: //www.asce.org/publications-and-news/civil-engineering-source/civil-engineerin g-magazine/article/2022/03/southern-california-city-seeks-to-end-reliance-on-i mported-water, March 2022.
- [36] B. Liberman, L. Eshed, G. Greenberg, Pulse flow RO the new RO technology for waste and brackish water applications, Desalination 479 (2020), 114336.
- [37] M. Li, A spatiotemporal model for dynamic RO simulations, Desalination 516 (2021), 115229.
- [38] L. Jiang, L.T. Biegler, V.G. Fox, Simulation and optimization of pressure-swing adsorption systems for air separation, AIChE J. 49 (2003) 1140–1157.
- [39] M. Li, Optimal plant operation of brackish water reverse osmosis (BWRO) desalination, Desalination 293 (2012) 61–68.
- [40] M. Li, B. Noh, Validation of model-based optimization of brackish water reverse osmosis (BWRO) plant operation, Desalination 304 (2012) 20–24.
- [41] M. Li, T. Bui, S. Chao, Three-dimensional CFD analysis of hydrodynamics and concentration polarization in an industrial RO feed channel, Desalination 397 (2016) 194–204.
- [42] M. Li, Residence time distribution in RO channel, Desalination 506 (2021), 115000.
- [43] M. Li, A unified model-based analysis and optimization of specific energy consumption in BWRO and SWRO, Ind. Eng. Chem. Res. 52 (2013) 17241–17248.
- [44] Y. Cohen, A. Rahardianto, T.K. Lee, Autonomous low energy consumption cyclic desalination systems. Desalination and water purification research and development program report no. 179, Bureau of Reclamation, Denver, CO, USA. https://www.usbr.gov/research/dwpr/reportpdfs/Report179.pdf, 2017.
- [45] A. Drak, M. Adato, Energy recovery consideration in brackish water desalination, Desalination 339 (2014) 34–39.